AGU PUBLICATIONS

Geophysical Research Letters

RESEARCH LETTER
10.1002/2014GL062442

Key Points:
- Snowpack displacement is quantified with terrestrial radar interferometry
- Temperature driven diurnal snow-glide cycles were recorded
- The precursor of a full-depth snow glide avalanche was monitored

Correspondence to:
R. Caduff,
caduff@gamma-rs.ch

Citation:
Caduff, R., A. Wiesmann, Y. Bühler, and C. Pielmeier (2015), Continuous monitoring of snowpack displacement at high spatial and temporal resolution with terrestrial radar interferometry, *Geophys. Res. Lett.*, *42*, 813–820, doi:10.1002/2014GL062442.

Received 7 NOV 2014
Accepted 14 JAN 2015
Accepted article online 16 JAN 2015
Published online 9 FEB 2015

Continuous monitoring of snowpack displacement at high spatial and temporal resolution with terrestrial radar interferometry

Rafael Caduff[1], Andreas Wiesmann[1], Yves Bühler[2], and Christine Pielmeier[2]

[1]GAMMA Remote Sensing AG, Gümligen, Switzerland, [2]WSL Institute for Snow and Avalanche Research SLF, Davos, Switzerland

Abstract Terrestrial radar interferometry is used in geotechnical applications for monitoring hazardous Earth or rock movements. In this study, we use it to continuously monitor snowpack displacements. As test site, the Dorfberg slope at Davos, Switzerland, was measured continuously during March 2014. The line of sight displacement was retrieved at a spatial resolution of millimeter to centimeter and a temporal resolution of up to 1 min independent of visibility. The results reveal several temperature-driven diurnal acceleration and deceleration cycles. The initiation of a small full-depth glide avalanche was observed after 50 cm total differential displacement. The maximum measured displacement of another differential glide area reached 43 cm/h without resulting in a full-depth avalanche even after a total measured differential displacement of 4.5 m. In regard of the difficulty to predict full-depth glide avalanches on the regional scale, the presented method has big potential for operational snow glide monitoring on critical slopes.

1. Introduction

Snow on the ground undergoes rapid changes such as temperature gradient metamorphism or mechanical compaction and deformation related to gravitational forces. Different deformation mechanisms are detected, such as the plumb-vertical-oriented settlement. On flat terrain, this is the only deformation component. Settlement rates depend on type, temperature, and water content of the snow. For dry snow, it ranges between 10 cm/d in new snow and 0.1 cm/d in old snow. On tilted surfaces, downslope shear deformations are present that result together with the vertical compression in creep deformation-directed downslope [*McClung and Schaerer*, 2006]. The creeping snowpack remains attached to the ground due to friction, while the upper layers of the snowpack move faster than the lower layers. The deformation shows an increase with an increase in temperature. If the ground surface is very smooth or the ground-to-snow interface is wet, the snowpack can also glide on a slope which is a third deformation mechanism. An overview of the relevant deformation components is presented in Figure 1.

Snow glide rates are between millimeters to a few meters per day. Glide cracks or full-depth glide avalanches may be the result of differential gliding movements [*Harvey et al.*, 2012]. This is a great concern for local and regional avalanche forecasting and safety personnel, because snow glide and full-depth glide avalanches are difficult to predict and can be very destructive, as large volumes of dense snow are moving. This may pose significant and prolonged hazard to roads, railroads, housing, and ski runs [*Peitzsch et al.*, 2012], as it was recently the case in the Alps. During winter of 2011/2012, Switzerland experienced a snow glide situation with at least a 30 year return period [*Bartelt et al.*, 2012b]. Major damage to infrastructure as well as two fatalities resulted due to increased snow glide and full-depth avalanche activity throughout the whole winter season [*Techel et al.*, 2013].

Forecasting glide snow avalanche activity based only on weather data are still difficult and relatively inaccurate [*Dreier et al.*, 2013]. Although the detection and the measurement of snow gliding are done for almost 100 years [*Höller*, 2014], continuous high-precision measurements could be made only at single locations [*In der Gand and Zupancic*, 1966; *Rice et al.*, 1996; *Wilson et al.*, 1996]. New techniques based on optical data [*Feick et al.*, 2012; *Hendrikx et al.*, 2012; *Van Herwijnen et al.*, 2013] or laser rangefinder measurements [*Hendrikx et al.*, 2010] can be applied only if the differential movement in the snowpack already led to tensile cracks and with clear visibility from the sensor to the target area. *Van Herwijnen et al.* [2013] have shown with time-lapse photography that glide snow avalanche releases correlate with periods of rapidly increasing glide rates.

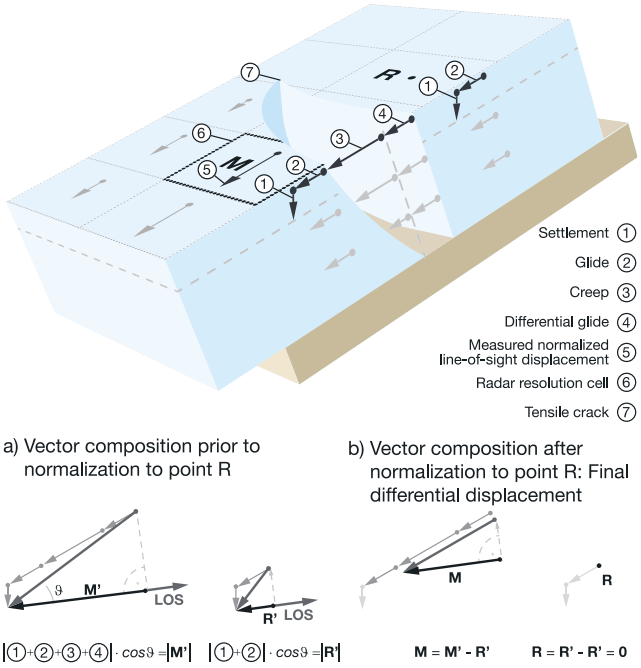

Figure 1. The snowpack block model shows snowpack displacement with already existing tensile crack. The different snowpack deformation components are numbered 1 to 4. The concept of interferometric measurements along line of sight is shown (a) prior and (b) after normalization to the reference point *R*. Normalization of measured LOS displacements (*M'*) is performed using a reference point close by (*R'*) that shows very similar large-scale properties. After subtraction of reference values, only differential movement along line of sight (*M*) remains.

No slope-wide measurements of snowpack displacement at an early stage of the movement, before a glide crack is visible, could be achieved so far. Localizing and mapping snow glide events and measuring glide rates independently of visibility and with high spatial and temporal resolution have great potential to improve the local forecasting of snow glide and full-depth glide avalanches and thereby support the protection of infrastructure and people.

Terrestrial radar interferometry has been proven to be a precise and reliable method for surface change detection related to mass movements in the geoscientific field [*Caduff et al.*, 2014]. We investigate its capability for the long-term detection and quantification of directed snowpack deformation on slope scale for the first time. The precision of the technique ranges from millimeters to centimeters without costly calibration. It was possible to measure the onset and end of significant differential snowpack displacement using coherent phase information continuously at all weather conditions with acquisition rates of up to one scene per minute. A temperature-dependent acceleration/deceleration cycle could be clearly shown. In one case, the acceleration led to a release of a small full-depth glide avalanche without the initiation of a visible tensile crack. A validation of the spatial distribution of measured snow gliding, its total deformation, and the occurrence of a small full-depth glide avalanche was performed using photogrammetry and time-lapse photography.

2. Measurement Scenario

2.1. Test Site

The test site Dorfberg is located near the city of Davos in the Swiss Alps. It is a southeast facing slope close to the ski area of Davos Parsenn. The observed area is about 6 km^2 large and reaches from 1560 m above sea level (asl) up to 2536 m asl. Slope angles reach up to 73°, and the mean slope angle lies close to 30°. The lower part of the slope is partially covered by dense coniferous forest. The upper part of the slope shows some snow-free steep rock outcrops. Snow-supporting structures made of steel are installed in the top area of the Dorfberg. The instrument was located in the valley bottom and directed toward the Dorfberg area. A map overview and a panoramic image from the test area are shown in Figure 2. The measurement campaign started on 31 January 2014 and ended on 24 April 2014.

2.2. Sensor

The measurements were taken by the GAMMA portable radar interferometer with a center frequency of 17.2 GHz (Ku band) and a chirp bandwidth of 200 MHz [*Werner et al.*, 2012]. It is a real aperture radar using slotted waveguide antennas with an aperture of 0.4°. The spatial resolution of the acquired images is 0.75 m in range and 7 m in azimuth at 1 km slant range. The instrument was installed in a radome for weather protection in front of the Institut für Schnee- und Lawinenforschung (SLF) facilities at the location indicated in Figure 2. Power and wired Ethernet connection was established using the SLF infrastructure on site.

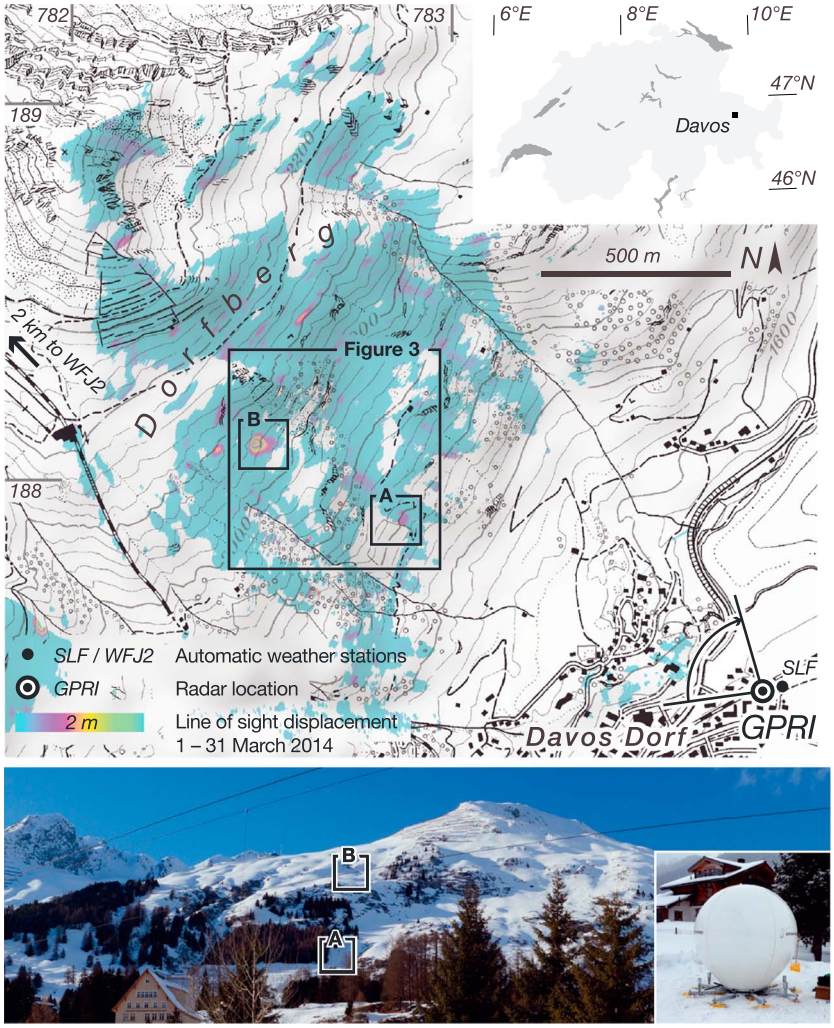

Figure 2. (top) Map overview of the test site and (bottom) panoramic view from the instrument location. (bottom right) The instrument was installed for weather protection in a radome of 2.4 m diameter. The map is colored with the cumulative 1 month line of sight displacement. The color scale is cyclic, where a single-color cycle indicates LOS displacement of 2 m. For area B, the surrounding shows LOS displacements close to zero, where toward the center of the deformation hot spot, LOS displacement of 4.5 m is shown by the addition of two single-color cycles. The details of the temporal evolution of A and B are discussed in the text.

2.3. Radar Acquisition Plan

Radar images are acquired by a rotation around the vertical axis of the antenna tower. The entire area of interest is covered by a scan angle of 80°. Azimuth line sampling was 0.1° (4 times oversampled regarding the antenna aperture of 0.4°). Maximum observed slant range was 3600 m. Radar image acquisition intervals were chosen according to the temporal decorrelation behavior of the observed snow slopes and were finally 5–30 min during nighttimes and up to 1 min during daytimes and a heavy snowfall event (indicated in Figure 3a). An overview of the acquisition intervals during the presented 1 month time series is shown in Figure 3b.

2.4. Data Processing

Raw data acquired according to the data acquisition schedule described above was preprocessed immediately after acquisition to single look complex format. Further, interferograms and coherence coefficients between the previous and the current acquisition were processed on site for the detection of sudden coherence changes induced by avalanches.

The interferometric analysis of continuous deformation was done by postprocessing. To reduce the amount of phase noise, interferograms were then adaptively filtered using the technique described in

Goldstein and Werner [1998]. A single coherence mask was applied for the whole data set to exclude areas covered with fast-decorrelating surface cover such as forest or areas covered by shrub vegetation.

Removal of atmospheric phase was performed with the approach described in *Caduff et al.* [2014] using spatial atmosphere estimation. The masked and filtered interferograms were then unwrapped in the spatial domain and converted to line of sight (LOS) displacements. This was done as well, if the coherence in the unmasked areas was below 0.8 for single interferograms. A critical assessment of all coherence maps revealed that only few (~50 scenes) were affected by sudden drops in the interferometric coherence caused mainly by free rider tracks, strong winds gusts, and avalanche events. The effects on the cumulative displacement maps were considered negligible for the desired accuracy of 1 cm displacement.

Single-displacement images were combined to a time series daily, respectively, and monthly displacement images were created showing the areas underlying slow deformation and the magnitude of the deformation. The images were converted from radar geometry to map geometry in Swiss coordinates (CH1903) using the terrain information of the swissALTI3D at 2 m pixel resolution. The final resolution of the map products is 1 m in east and in north direction to keep most of the information resulting from the high radar range resolution.

For selected points, a total time series of the deformation (Figure 3a) and the spatial coherence (Figure 3b) was extracted between 1 and 31 March 2014. It shows the temporal behavior of the deformation and the coherence. The coherence values of points B.2 and B.3 showed a drastic reduction on 10 and 11 March during several hours in the daytime. Since the interferometric coherence remained low for several hours, sudden mechanical changes such as avalanches could be excluded as cause for the decorrelation. Single interferograms showed that the area is consistent with the area previously determined as deforming. During the nights, the interferometric coherence stabilized again, so that the single-image approach was again feasible. To prevent false solutions for the automated unwrapping of area B induced by the low coherence, single interferograms were averaged (12–30 scenes per hour at the time indicated as dashed line in the displacement diagram of Figure 3a). Phase noise could be reduced and fringe visibility was enhanced, so that a spatial unwrapping process could be performed successfully. However, due to the very steep phase gradients during times of maximum deformation rates, the unwrapping result may be underestimated by 1–2 phase cycles (~8–16 mm) that is propagated to the estimation of the integrated hourly displacement. Finally, plotted point deformations were normalized using corresponding points outside this area with similar snowpack characteristics to get rid of homogenously distributed phase changes as indicated in Figure 1. The presented deformation rates are expressed in LOS only. Assuming gravity-driven, surface-parallel flow, coverage of 97% and 84%, respectively, of the total deformation in points A and B is determined.

A snowfall event between 22 and 24 March 2014 is included as well in the cumulative displacement. Here 55 cm of new snow accumulation was recorded (Figure 3c). Relative phase changes during this time occurred, but the effect causing the phenomenon was not investigated in detail.

2.5. Reference Data

Cotemporal weather data (relative humidity, snow depth, air temperature, and snow surface temperature) is available in 30 min intervals from two automatic weather stations (SLF and Weissfluhjoch (WFJ2)). Data are shown in Figure 3c. The weather station SLF is located at a distance of 50 m from the instrument at an elevation of 1560 m asl. The second weather station (WFJ2) is not in direct sight of the radar but about 2 km up valley behind the crest of the Dorfberg at an elevation of 2540 m asl. Weather and snowpack data were related to phases of accelerated snowpack displacement.

For the validation of snowpack displacement and avalanche activity, a fixed digital camera, installed at SLF facility, was imaging the Dorfberg area in 2 min intervals. The image size is 2592×1944 pixels and a 35 mm equivalent focal length of 51 mm. Additional image sets of the test site were acquired with 4912×3264 pixels size and with 35 mm focal lengths between 24 and 246 mm from different positions. These image sets were calibrated with structure-from-motion technique [*James and Robson*, 2012] using the software "Photoscan v10.0 pro" from Agisoft together with the webcam images. Image calibration was later used for the validation of radar measurements.

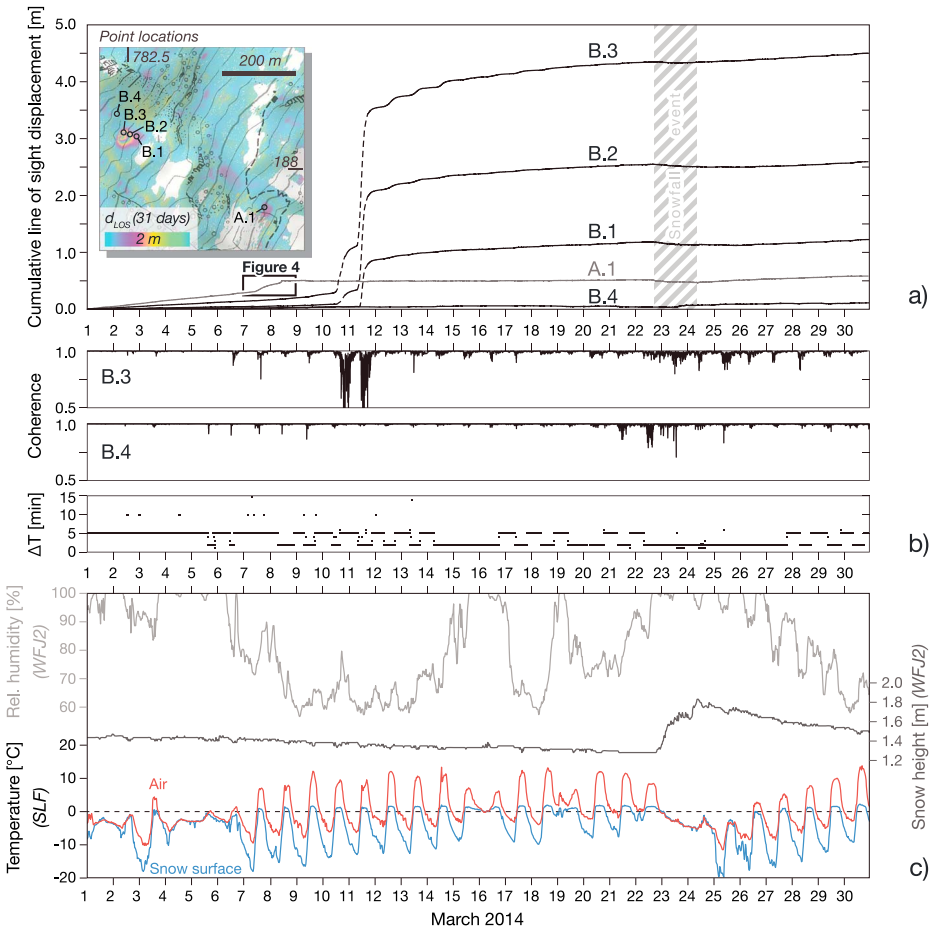

Figure 3. (a) Temporal differential displacement history for selected points (A and B) indicated in the detail map. The location of the detail view is indicated in Figure 2. The details about the determination of the cumulative displacement are given in the text. (b) Information for coherence at the indicated point locations and the time intervals of all single acquisitions (ΔT). (c) Weather data: relative humidity, air and snow temperature from station SLF, and snow height data from station WFJ2. The locations of the two stations are indicated in Figure 2.

3. Results and Validation

Results obtained after the postprocessing show the spatial and the temporal evolution of the snow cover LOS displacement during 1 month (1 to 31 March 2014). The cumulative sum of the displacement over the entire test site for the presented period is mapped in Figure 2. The results reveal several areas showing deformation toward the sensor. Two areas showing different magnitudes and snow mechanical properties are marked with A and B in Figure 2 and are analyzed in detail in the following section.

The temporal evolution of point A.1 shows more or less constant velocity at the beginning of the time series (Figure 3a). On 7 March 2014, acceleration was recorded beginning at 11:00 UTC followed by a deceleration beginning at 18:00 UTC. The next day, acceleration was observed again, starting at 09:00 UTC until an avalanche released shortly before 11:36 UTC. The LOS displacement rate prior to the release was 2.86 cm/h, and the total observed differential displacement distance was 50 cm until release. The deformation history of a point in the release area as well as the webcam images before and after the release are shown in Figure 4. The event is recorded as well in the coherence image showing the extent of the avalanche including the release area and the accumulation area in webcam geometry. The technique for reprojection of radar data onto the webcam image is presented in *Caduff and Rieke-Zapp* [2014] and shows for this case a projection accuracy of 2 to 4 m in object space. The recorded extent of the decorrelated area fits well with the changes observed by the webcam. The snowpack was released from a 25 m wide initiation zone. The total area affected by the glide was ~1500 m^2.

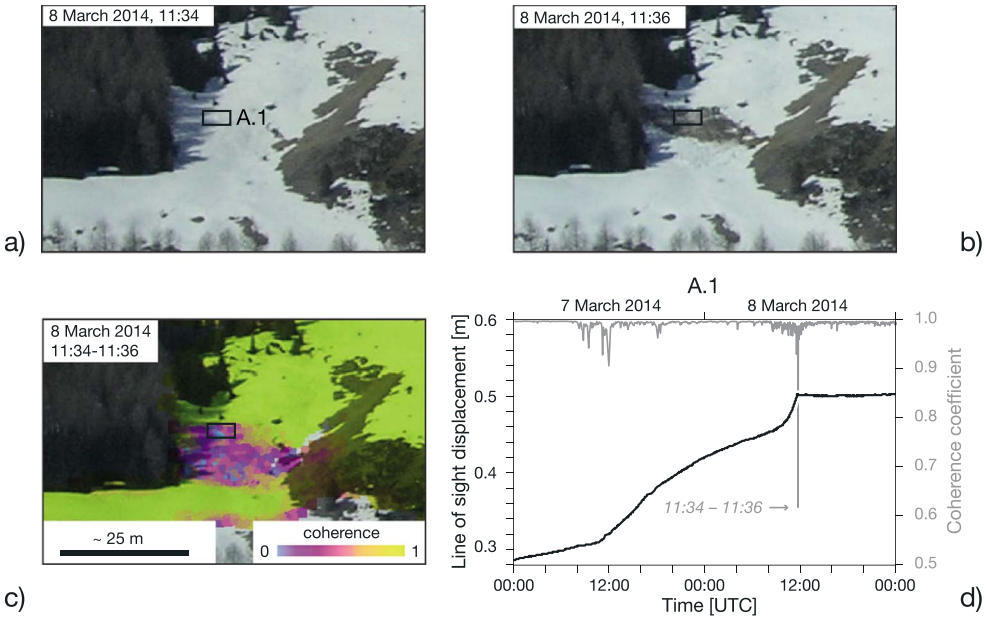

Figure 4. Webcam images (a) before and (b) after a spontaneous snow glide event (Fotos: A. Van Herwijen/SLF). (c) Interferometric decorrelation map overlaid over webcam image showing the decorrelation in the initiation and accumulation zone induced by the event. (d) Line of sight deformation and interferometric coherence history of point A.1. (The footprint from which the time series values for Figure 4d were extracted is indicated in Figures 4a–4c as black rectangle).

Area B showed the highest maximum LOS displacement rate of up to 43 cm/h detected on 11 March 2014 at 12:00 UTC at point B.3. Total cumulative LOS displacement in the presented 1 month period was maximum 4.5 m. Figure 3a shows the deformation of the three points in the affected area (B.1, B.2, and B.3) and for one control point outside of the main creeping area (B.4).

A validation with webcam imagery and terrestrial photos was done using the same technique as described above. The mapped extent of the deformation measured on 13 March 2014 fits the detail image of area B (Figure 5). At this time, a tension crack opening of 4.2 m uncovering the soil could be determined using the structure-from-motion technique. At the lower part of the area, bulging is a sign for the compression zone of the gliding snow. A vertically oriented snow thrust, left of the center of the deformation, shows a direction change within the deformation. The detailed daily displacement maps in Figure 5 show the opening of the tension crack (dashed line) in a slightly rotational structure (arrow). The spatial distribution of the displacement rates shows that on 10 March 2014, the tension crack is opening. This is visible on the very steep gradient of deformation in the upper part. Note that color scales are normalized to maximum deformation per day. Values below 10% of the maximum displacement were shown as 0 (blue).

4. Discussion and Conclusion

We investigated the applicability of terrestrial radar interferometry for slope-wide snow displacement monitoring. The promising results may lead to better understanding in a slope-wide observation of snowpack displacement behavior. The distribution of the differential gliding areas on a slope, the temporal evolution of the deformation rates, and the kinematics of the snowpack deformation (such as initiation of glide cracks or changes in the extent of the deformation) can be determined as accurately measured in near real time. The total area of the gliding zone can be derived providing an estimate of the size of a potential full-depth glide avalanche and facilitate mitigation methods. It turned out that the forecasting of glide snow avalanche release solely from acceleration rates is inconclusive, since for one case with great acceleration rates in the snowpack displacement, no avalanche release occurred. Whether the avalanche releases or the snowpack regains stability depend also on the snow mechanical properties, which change during the process. Hence, combining known properties, weather data and displacement information can enhance avalanche predictions.

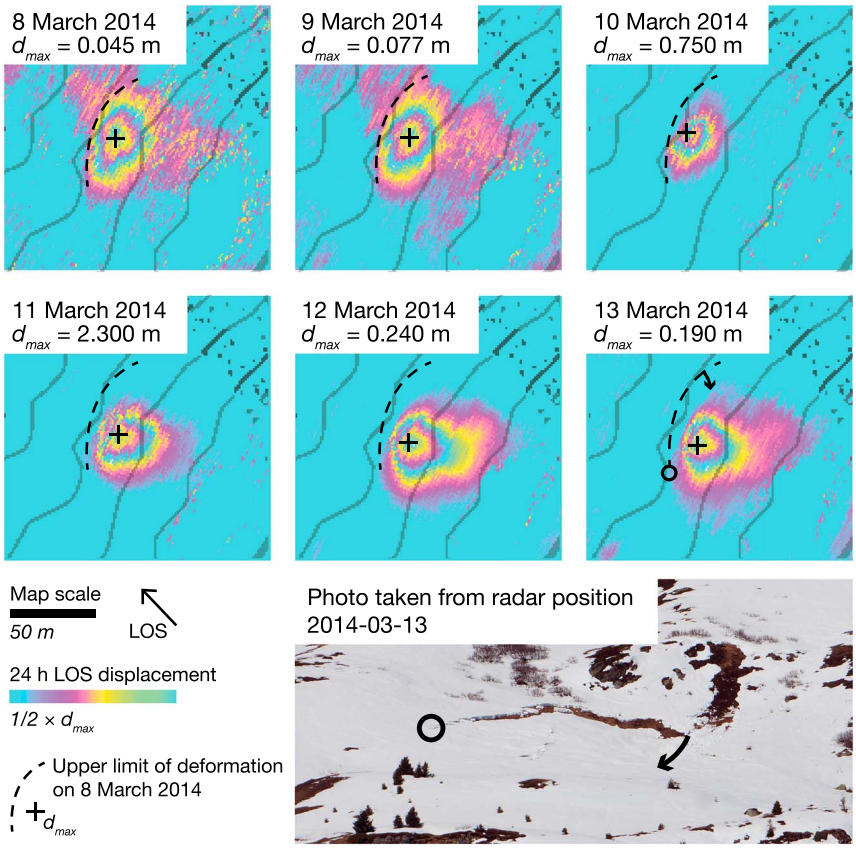

Figure 5. Spatial distribution of daily cumulative line of sight (LOS) displacement at B (location indicated in Figure 2). The radar look direction with respect to the map views is indicated as LOS. The map samples show situation before, during, and after the maximum daily displacements measured at 11 March 2014. The color scale is normalized to the daily maximum displacement (d_{max}) indicated as cross in the maps. One color cycle represents $0.5 \times d_{max}$ of a single day. Displacement values $<10\%$ of d_{max} including radar shadow and decorrelating areas set to 0 (blue). The change in the extent of the deforming area and the location of the d_{max} are visible as well as the initiation of a tensile crack (indicated as dashed line).

Some metrological questions still remain open. One question concerns the phase center and thus related the penetration depth of the microwaves at Ku band in the different snow types. As discussed by *Mätzler* [1998], penetration depths at microwave frequencies are dependent on snow properties, especially on the liquid water content. The presence of dominant layers such as crusts and coarse-grained hoar layers also has an impact on the location of the phase center at Ku band frequencies. A shift of the phase center can be confused with the displacement signal if the interferometric coherence is reasonably high between succeeding acquisitions. Such an effect of rapid changes in backscatter could be observed on a daily basis close to the time of sunrise. As a consequence, changes in the measured phase due to changes of the penetration depth may bias the measured LOS displacement, if no normalization is performed.

In principle, the presented methodology should also be applicable at other frequency bands. As a dual-frequency experiment at 5.3 GHz and 35 GHz, respectively, shows, lower frequencies should also perform well during wet-snow conditions since the main phase contribution derives from within the snowpack [*Wiesmann et al.*, 2007]. For dry snow, the methodology will be hampered due to the potentially dominating ground contribution. Higher-frequency bands are more sensitive to volume scattering and should also perform well in dry-snow conditions as the experiment shows. The limiting parameter will be the displacement rate causing unwrapping issues due to the higher sensitivity on displacement at higher frequencies. A dual-frequency system might answer open questions regarding the location of the phase center and the range of snow conditions suited for the presented methodology and might help with phase unwrapping issues.

The questions, if the measured displacement is biased by the change in the penetration depth and if the snowpack displacement is not homogeneously distributed vertically, are linked with the uncertainty about

the location of the phase center at the used frequency. This might be the case for creep displacement, where the displacement rate close to the snow surface is higher than close to the bottom layer of the snowpack. As presented, this is of no concern if the snowpack is gliding at full depth. Additionally, absolute calibration of the measured snowpack deformation using different methodologies on selected locations may help to separate creep from glide movements.

The presented measurement methods can improve the understanding of snowpack displacement and the formation of full-depth glide snow avalanches. Therefore, enhanced model predictions of present models [*Leitinger et al.*, 2008; *Mitterer and Schweizer*, 2012; *Bartelt et al.*, 2012a] and the determination of the main driving forces including the deformation-related stress field on a slope scale can be achieved even if no initial glide crack has formed prior to the avalanche release. The method offers as well an all-weather real-time determination of the snow glide and avalanche activity on a slope scale. This is expected to be helpful for avalanche warning and in particular for monitoring endangered infrastructure during hazardous gliding snow situations such as 2012 in Switzerland. The proposed method offers the possibility to determine the exact location of gliding areas over entire slopes and may be used in the future for early warning purposes. The method could be of help as well for choosing the time of the lowest basal friction indicated by high displacement rates. As proposed by *Bartelt et al.* [2012a], success for blasting the stauchwall of a snow glide and therefore releasing the snow slab is highest during times with lowest basal friction.

Acknowledgments
Data acquisition was partially funded by ESA ARTES 20 IAP "Improved Alpine Avalanche Forecast Service AAF" contract 4000108853/13/NL/NR. Topographic map (PK25) and terrain height information (swissALTI3d, 2 m) used in the figures and for georeferencing radar data are ©swisstopo. The webcam imagery, used to validate presented data, is through the courtesy of A. Van Herwijnen of SLF.

The Editor thanks an anonymous reviewer for assisting in the evaluation of this paper.

References

Bartelt, P., T. Feistl, Y. Bühler, and O. Buser (2012a), Overcoming the stauchwall: Viscoelastic stress redistribution and the start of full-depth gliding snow avalanches, *Geophys. Res. Lett.*, *39*, L16501, doi:10.1029/2012GL052479.

Bartelt, P., C. Pielmeier, S. Margreth, S. Harvey, and T. Stucki (2012b), The underestimated role of the Stauchwall in full-depth avalanche release, in *Proceedings of the International Snow Science Workshop*, pp. 127–133, Anchorage, Alaska, 16–21 Sept.

Caduff, R., and D. Rieke-Zapp (2014), Registration and visualization of deformation maps from terrestrial radar interferometry using photogrammetry and structure from motion, *Photogram Record.*, *29*(146), 167–186, doi:10.1111/phor.12058.

Caduff, R., F. Schlunegger, A. Kos, and A. Wiesmann (2014), A review of terrestrial radar interferometry for measuring surface change in the geosciences, *Earth Surf. Process. Landf.*, doi:10.1002/esp.3656.

Dreier, L., C. Mitterer, S. Feick, and S. Harvey (2013), The influence of weather on glide snow avalanches, in *Proceedings of the International Snow Science Workshop 2013*, pp. 247–252, Grenoble, France, 7–11 Oct.

Feick, S., C. Mitterer, L. Dreier, S. Harvey, and J. Schweizer (2012), Automated detection and monitoring of glide snow events using satellite based optical remote sensing and terrestrial photography, in *Proceedings of the 2012 International Snow Science Workshop*, Anchorage, pp. 603–609.

Goldstein, R. M., and C. L. Werner (1998), Radar interferogram filtering for geophysical applications, *Geophys. Res. Lett.*, *25*(21), 4035–4038, doi:10.1029/1998GL900033.

Harvey, S., H. U. Rhyner, and J. Schweizer (2012), *Lawinenkunde*, pp. 192, Bruckmann, München, Germany.

Hendrikx, J., E. H. Peitzsch, and D. B. Fagre (2010), A practitioner's tool for assessing glide crack activity, in *Proceedings of the 2010 International Snow Science Workshop*, pp. 395–396, Lake Tahoe, Calif. 17–22 Oct.

Hendrikx, J., E. Peitzsch, and D. Fagre (2012) Time-lapse photography as an approach to understanding glide avalanche activity, in *Proceedings of the 2012 International Snow Science Workshop*, pp. 872–877, Anchorage Alaska.

Höller, P. (2014), Snow gliding and glide avalanches: A review, *Nat. Hazards*, *71*(3), 1259–1288, doi:10.1007/s11069-013-0963-9.

In der Gand H., and M. Zupancic (1966), Snow gliding and avalanches, IAHS-Publ. 69, pp. 230–242.

James, M. R., and S. Robson (2012), Straightforward reconstruction of 3-D surfaces and topography with a camera: Accuracy and geoscience application, *J. Geophys. Res.*, *117*, F03017, doi:10.1029/2010JF002289.

Leitinger, G., P. Höller, E. Tasser, J. Walde, and U. Tappeiner (2008), Development and validation of a spatial snow glide model, *Ecol. Model.*, *211*(3), 363–374.

Mätzler, C. (1998), Microwave properties of ice and snow, *Solar Syst. Ices Part I Astrophys. Space Sci. Lib.*, *227*, 241–257, doi:10.1007/978-94-011-5252-5_10.

McClung, D., and P. Schaerer (2006), *The avalanche handbook*, 3rd ed., pp. 342, Mountaineers, Seattle Wash.

Mitterer, C., and J. Schweizer (2012), Toward a better understanding of glide snow avalanche formation, in *Proceedings of the 2012 International Snow Science Workshop*, pp. 610–616, Anchorage Alaska.

Peitzsch, E., J. Hendrikx, D. Fagre, and B. Reardon (2012), Examining spring wet slab and glide avalanche occurrence along the Going-to-the-Sun Road corridor, Glacier National Park, Montana, USA, *Cold Regions Sci. Tech.*, *78*, 73–81, doi:10.1016/j.coldregions.2012.01.012.

Rice, B., D. Howlett, and R. Decker (1996), Preliminary investigations of glide/creep motion sensors in Alta, Utah, in *Proceedings of the International Snow Science Workshop 1996*, pp. 189–194, Banff, Canada.

Techel, F., C. Pielmeier, G. Darms, M. Teich, and S. Margreth (2013), Schnee und Lawinen in den Schweizer Alpen, Hydrologisches Jahr 2011/12, WSL Ber, 5: 118 p.

Van Herwijnen, A., N. Berhod, R. Simenhois, and C. Mitterer (2013), Using time-lapse photography in avalanche research, in *Proceedings of the International Snow Science Workshop 2013*, pp. 950–954, Grenoble, France, 7–11 Oct.

Werner, C. L., A. Wiesmann, T. Strozzi, A. Kos, R. Caduff, and U. Wegmüller (2012), The GPRI multi-mode differential interferometric radar for ground-based observations, paper presented at 9th European Conference on Synthetic Aperture Radar, EUSAR, 23–26 April, Nuremberg, Germany.

Wiesmann, A., T. Strozzi, C. Mätzler, C. Werner, U. Wegmüller, and M. Santoro (2007), Backscatter measurements of snow cover, in *Proceedings of Retrieval of Bio- and Geophysical Parameters from SAR Data for Land Applications*, Bari, Italy, 25–28 Sept.

Wilson, A., G. Statham, R. Bilak, and B. Allen (1996), Glide avalanche forecasting, in *Proceedings of the International Snow Science Workshop 1996*, pp. 129–131, Banff, Canada.